

# REMOTE SENSING OF SNOW WETNESS IN ROMANIA BY SENTINEL-1 AND TERRA MODIS DATA

R. SOLBERG<sup>1</sup>, A.-B. SALBERG<sup>1</sup>, Ø. DUE TRIER<sup>1</sup>, Ø. RUDJORD<sup>1</sup>,  
G. STANCALIE<sup>2</sup>, A. DIAMANDI<sup>2</sup>, A. IRIMESCU<sup>2</sup>, V. CRACIUNESCU<sup>2</sup>

<sup>1</sup>Norwegian Computing Center (NR), P.O. Box 114 Blindern, NO-0314 Oslo, Norway,  
E-mail: rune.solberg@nr.no

<sup>2</sup>Romanian National Meteorological Administration (NMA), 97 Soseaua Bucuresti-Ploiesti,  
RO-013686 Bucharest, Romania  
E-mail: gheorghe.stancalie@meteoromania.ro

*Received March 19, 2017*

*Abstract.* Snow monitoring is essential for prediction of flooding due to rapid snowmelt, to provide snow avalanche risk forecasts and for water resource management – including hydropower production, agriculture, groundwater and drinking water. Sentinel-1 C-band SAR is sensitive to presence of wet snow and can be used to binary snow-wetness classification. Wet-snow mapping into more categories has been demonstrated in the past by using MODIS data. The combination of surface temperature and the temporal development of the effective snow grain size are used to infer approximately how wet the snow is.

*Key words:* remote sensing, snow wetness mapping, optical, SAR, Sentinel-1, MODIS.

## 1. INTRODUCTION

Snow is a key element of the water cycle. Seasonal snow is characterized by high temporal variability. The variations at daily-to-seasonal time scales are superimposed to long-term trends in the cryosphere, which have been observed during the last decades and are attributed to climate change [1, 2]. Satellite sensors are the optimum tools for cryosphere monitoring. Accurate observations of snow properties and state are of great interest for hydrology, meteorology and climate change research and applications.

The overall objective of the EEA Grants SnowBall project, which carried out the work presented here, is to explore and develop methodology supporting the vision of developing a future service providing Romanian national authorities with hind-cast and real-time snow and avalanche information from earth observation data. Project work includes development of algorithms and implementation of a prototype snow monitoring system using Sentinel-1 and -3 satellite data for snow surface wetness mapping.

This paper presents the algorithm development and preliminary validation results from the test sites in Romania for the 2015 snow season. The validation was limited to comparison with air temperature as available for this season.

The primary satellite data sources for our algorithms are Sentinel-3 for optical and Sentinel-1 for *synthetic aperture radar* (SAR). Since Sentinel-3 will only deliver data operationally from early 2017, we have used Terra MODIS data for the algorithm development and validation so far.

Sentinel-3A, launched 16 February 2016, has two optical instruments. The *Ocean Land Colour Instrument* (OLCI) is based on the heritage from ENVISAT's *Medium Resolution Imaging Spectrometer* (MERIS) instrument. The OLCI operates across 21 wavelength bands from ultraviolet to near-infrared and uses optimized pointing to reduce the effects of sun glint. The swath width is 1270 km, and the spatial resolution 300 m.

The *Sea Land Surface Temperature Radiometer* (SLSTR) is based on the heritage from ENVISAT's *Advanced Along-Track Scanning Radiometer* (AATSR). The SLSTR uses a dual-viewing technique and operates across nine wavelength bands providing better coverage than AATSR because of a wider swath width (1675 km for the nadir view angle). The sensor has three bands in the visual and near-infrared (555, 659 and 865 nm), three in the mid infrared (1.38, 1.61 and 2.25  $\mu\text{m}$ ) and three in thermal infrared (3.74, 10.85 and 12  $\mu\text{m}$ ). The spatial resolution is 500 m at visible and infrared and 1 km at thermal domain.

Sentinel-1 carries a C-band *Synthetic Aperture Radar* (SAR) building on ESA's and Canada's heritage in SAR systems from ERS-1, ERS-2, Envisat and Radarsat. Sentinel-1A was launched 3 April 2014, and Sentinel-1B 25 April 2016. The satellites have repeat cycles of 12 days. The C-band SAR operates in four modes: 1) Strip Map Mode (SM); 2) Interferometric Wide Swath (IW); 3) Extra-Wide Swath Mode (EW); and 4) Wave-Mode (WV). Over land the primary, conflict-free, mode is IW with VV+VH polarizations. The resolution of the IW-mode depends on whether the product is *single-look complex* (SLC) or *ground range detected* (GRD) and number of looks. The SLC range-azimuth pixel spacing is  $2.3 \times 17.4$  m, whereas for the IW GRD product, the pixel spacing is  $10 \times 10$  m with number of looks equal to  $5 \times 1$ .

The first validation dataset was collected in winter/spring 2015 in Romania. Precursor algorithms and products for wet snow were previously tested in the Jotunheimen site in Norway by NR, and later demonstrated and applied in the whole country of Norway. Jotunheimen is the highest part of the Scandinavian Mountains, and is located in central southern Norway. The SnowBall algorithms are now validated in Jotunheimen, and subsequently in the Bucegi mountain Sinaia region in Romania, part of the Southern Carpathian. The Romanian sites for diagnostic data collection and algorithm cal/val have been selected as the upper sector of the Arges and Ialomita river catchments with altitudes of about 500 to

2500 m. There are eight meteorological stations in the area, all operated by the *National Meteorological Administration* (NMA).

## 2. ALGORITHMS

### 2.1. OPTICAL

The ideal approach for retrieval of snow surface wetness based on optical data would be to measure the liquid water contents in the snow, like that proposed and demonstrated in [3]. However, this would require an imaging spectrometer with optimally located spectral bands for measuring liquid-water molecular absorption features. Such sensors are currently not available in satellites, only as experimental sensors in aircrafts. Our aim has been to develop an algorithm to be used operationally based on satellite data.

Experiments with snow wetness algorithms have confirmed that a combination of snow surface skin temperature and snow grain size, analysed in a time series of observations, can be used to infer wet snow, including giving an early warning of snowmelt start [4]. The temperature observations give a good indication of where wet snow potentially could be present, but are in themselves not accurate enough to provide sufficiently strong evidence of wet snow. However, if a rapid increase in the effective snow grain size is observed simultaneously with a snow surface temperature of approximately 0 °C, then this is a strong indication of a wet snow surface.

#### **The snow surface temperature algorithm**

The *surface temperature of snow* (STS) algorithm is based on an approach proposed in [5]. In a comparison study [6], this algorithm was identified as one of the best single-view techniques for retrieval of STS for polar atmospheres, and it can be applied with several sensors of moderate resolution, like MODIS, AVHRR, AATSR and OLCI/SLSTR.

The absorption of the radiation in the atmosphere depends on the wavelength, and the difference between the brightness temperatures in two channels will therefore yield information about the atmospheric attenuation [7, 8]. The split-window technique aims at eliminating the atmospheric effects by utilizing this difference. The surface temperature  $T$  is estimated as a weighted sum (or difference) of the brightness temperatures observed. The split-window equation utilizes  $T_{11}$  measured at 11  $\mu\text{m}$  (MODIS band 31, SLSTR band 7) and  $T_{12}$  measured at 12  $\mu\text{m}$  (MODIS band 32, SLSTR band 8):

$$T = b_0 + b_1 T_{11} + b_2 T_{12} \quad (1)$$

The split-window technique is only sensitive to the effect of the atmospheric water vapour, and not to other atmospheric gases or aerosols. The atmospheric influence on the split-window equation depends on the composition of the atmosphere, and the method must therefore be calibrated for different atmospheres.

Coll's modification [8] to the split-window algorithm was proposed in order to avoid the need of several calibration sets. It is a global non-linear equation for global-scale application. Derivation of regionally optimized linear algorithms has been demonstrated for mid-latitude conditions, but not for colder atmospheres. Coll's equations are given by:

$$T = T_{11} + A(T_{11} - T_{12}) + B \quad (2)$$

$$A = b_0 + b_1(T_{11} - T_{12}) \quad (3)$$

where:  $b_0 = 1.00$ ,  $b_1 = 0.58$ ,  $B = 0.51$ .

Key's algorithm [5] is a modification of the simple split-window technique. An additional correction term addresses the variation of the view angle  $\theta$  along a scan line and its effect of the atmospheric path length. The algorithm expresses the surface temperature as:

$$T_s = b_0 + b_1 T_{11} + b_2 (T_{11} - T_{12}) + b_3 (T_{11} - T_{12})(\sec \theta - 1) \quad (4)$$

The calibration coefficients depend on the temperature interval and the satellite sensor.

### The snow grain size algorithm

For *snow grain size* (SGS) we have used a normalized grain size index based on work in [9] and followed by experiments in [10]. MODIS bands 2 and 7 have been used as this index has been shown to be less sensitive to snow impurities.

The original algorithm proposed in [9] was based on Landsat Thematic Mapper (TM) data. The problem of radiometric terrain effects, the influence of slopes on the reflected light, is minimized by using ratios between two channels as an index for grain size. A number of ratios of the form:

$$R_{ij} = \frac{TM_i - TM_j}{TM_i + TM_j} \quad (5)$$

were tested. We selected the  $R_{47}$  as the best. In [10] it was reported that the measured data matches the theoretical curves well. The ratio approach is a simple method. Signals from two channels are sufficient and information about the terrain is not needed (as it is with several other methods). Studies of calculated grain size from the  $R_{47}$  ratio show that the index is well suited for monitoring the changes in grain size due to precipitation and temperature changes. The index increases with increasing temperature and gets a lower value when new snow has fallen.

The grain size index for snow for MODIS data lies typically between 0.7 and 1.0. Bare ground of different kinds gives lower index values. 0.7 is not an exact threshold value for snow. Somewhere around 0.7 the index shows that there is probably some snow on the ground. To be sure that the index represents snow grain size, we use a fractional snow cover retrieval algorithm in addition to check that the ground is fully snow covered.

### The snow surface wetness algorithm

The approach is to infer wet snow from a combination of measurements of STS and SGS in a time series of observations materialised when NR analysed *in situ* and MODIS data for various snow parameters in test sites in Jotunheimen. An example of the temporal development of data from the winter and spring season 2003 is shown in Fig. 1 for the two test sites in Jotunheimen. Note the rapid increase of SGS at one site (Valdresflya) when the air temperatures approaches and reaches 0 °C level from below. The STS values follow the air temperatures exactly as expected.

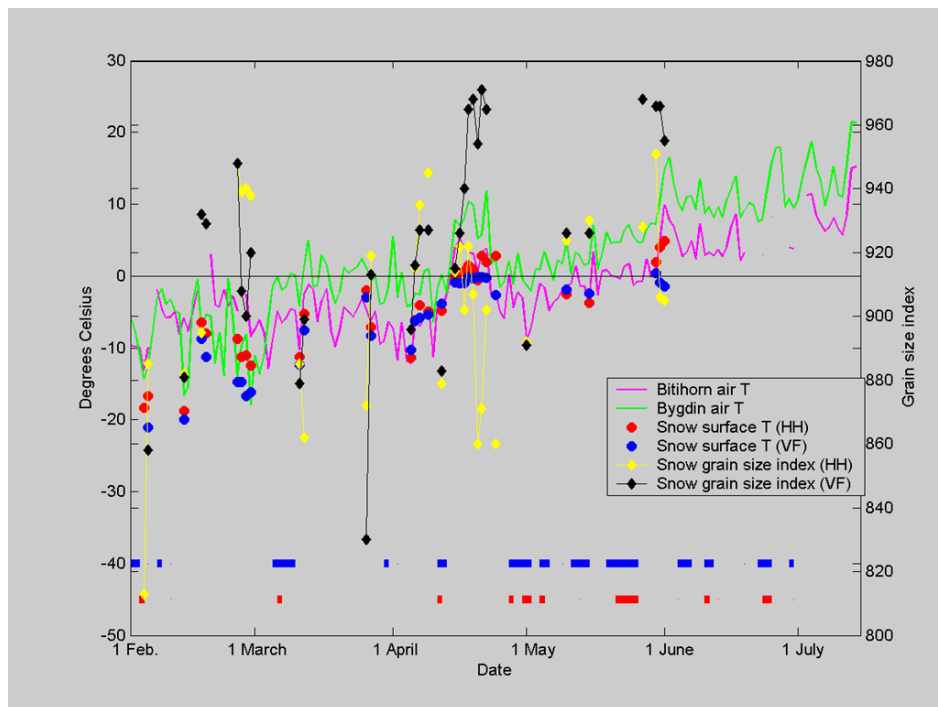


Fig. 1 – STS and SGS retrieved from MODIS data at Valdresflya (VF) and Heimdalshø (HH), Jotunheimen, Norway, in winter/spring 2003 (dotted lines). Temperatures from two weather stations are also shown (solid lines).

The process driving the SGS increase is snowmelt metamorphism. It typically takes place in the spring when snowpack temperatures are close to 0 °C. During daytime the air temperature increases to well above 0 °C and the snow surface starts to melt. In the late afternoon, evening and nights the temperature falls and the snow surface refreezes. During the melting, smaller grains melt first, and liquid water appears in the upper layer of the snowpack. The bonds between the snow grains are typically destroyed, and the remaining snow grains are covered by a layer of liquid water. When the temperature cools again, the liquid water freezes and the snow grain size of the remaining grains increases due to the liquid water added. From this processes, a melting snowpack typically has an aggregation of rounded grains of 1–2 mm (corn snow). Note that snowmelt metamorphism also might take place due to rain. Liquid water from rain percolates downward in the snowpack and refreezes.

Based on the type of observations shown above, we developed an approach to infer categories of *snow surface wetness* (SSW) from a combination of measurements of STS and SGS in a short time series. The temporal behaviour of STS and in particular SGS let us infer the current snowmelt stage the snow surface is within from the multi-temporal observations. We developed a decision-tree approach for classification into the snow wetness categories. The decision boundaries were tuned based on calibration data from test sites in Jotunheimen (*in situ* measurements of liquid water in the snow surface and weather station air temperature measurements) [4, 11].

A simplified version of the algorithm applied is expressed below (pixel indexing has been skipped for clarity; *MSSW* is time-series multi-sensor snow surface wetness):

```

if  $SGS(\text{today}) - SGS(\text{recently}) > SGStresh$  AND  $-2 < STS(\text{today}) < 1$  then  $MSSW = WET\_SNOW$ 
else if  $SGS(\text{today}) < BareGroundSGStres$  then  $MSSW = BARE\_GROUND$ 
else if  $STS(\text{today}) > 1$  then  $MSSW = BARE\_GROUND$  else  $MSSW = DRY\_SNOW$ .

```

The decision tree further refines *MSSW* into categories of wet snow. The algorithm also illustrates how bare ground is inferred from temperature observations above 0 °C and a rapidly developing negative gradient for SGS (both due to appearance of bare ground patches at the sub-pixel level).

Experiments with the snow wetness algorithm have confirmed that the approach of combining STS and SGS, analysed in a time series of observations, can be used to infer wet snow, including giving an early warning of snowmelt start. Air temperature measurements from meteorological stations confirm the maps produced in general. A potential problem sometimes observed is related to clouds. Non-detected clouds or cloud fractions within a pixel will usually decrease the temperature retrieved. One should be aware of this potential problem with partly cloudy SSW maps.

## 2.2. SYNTHETIC APERTURE RADAR

SAR imaging systems allow for imaging through clouds, and because SAR is an active system, day and night imaging is possible. Due to the nature in which microwaves interact with the surface features the information in the backscattered radar signals can be indicative of moisture content, salinity and physical characteristics (shape, size, orientation).

Using SAR to map the snow cover has some limitations. A dry snowpack has minor influence on the SAR signals, and the reflected signals are dominated by the contribution of the snow/ground interface. However, when the snow is wet, the radar signals cannot penetrate the snow, and the backscattered signal is dominated by the contribution from the air/snow interface. The reflected signal is often lower from areas covered with wet-snow, compared to snow-free or dry snow.

Wet snow may therefore be mapped in a SAR image by comparing the backscatter coefficient values with corresponding backscatter coefficients from a reference image obtained at snow-free or dry snow conditions [12]. Hence, the algorithm for mapping wet snow is based on change detection using ratios of wet snow *versus* snow-free (or dry snow) surfaces.

To avoid the need for reference images in the same imaging geometry, we have implemented an alternative method for mapping wet snow areas. This is based on the ‘flattening-gamma’ radiometric terrain correction approach in [13]. Without treatment, the hill-slope modulations of the radiometry threaten to overwhelm weaker thematic land-cover induced backscatter differences, and comparison of backscatter from multiple satellites, modes, or tracks loses meaning. The ‘flattening-gamma’ SAR methodology suppresses a large part of the brightness variation in the SAR images caused by terrain variation, and may therefore provide a proper treatment to the hill-slope modulations. The ‘flattening-gamma’ products have shown great potential for improving SAR-based mapping of wet snow in mountainous areas, *e.g.* at time of spring snowmelt. However, the quality of the ‘flattening-gamma’ products depends strongly on the quality of the DEM and precision of the geocoding.

### **The wet snow mapping algorithm**

Wet snow may be detected in a SAR image by comparing backscatter coefficient values with corresponding backscatter coefficients from a reference image obtained at snow free or dry snow conditions [12]. Hence, the algorithm for mapping wet snow is based on change detection using ratios of wet snow *versus* snow-free (or dry snow) surfaces.

To avoid requiring reference images to be in the same imaging geometry, we have implemented the alternative method based on the ‘flattening-gamma’ radiometric terrain correction approach [13].

The steps in the wet snow mapping algorithm may be summarized as follows:

1. Conversion of the SAR data (digital numbers) to gamma naught.
2. Multi-looking to reduce speckle noise. The number of looks we apply depends on the desired output resolution. We have applied 6×6 looks (corresponding to a desired pixel spacing of 50 × 50 m).
3. Conversion to terrain-corrected gamma naught (‘flattening gamma’) backscatter normalization.
4. Computation of layover and shadow masks.
5. Geocoding using the range-Doppler algorithm.
6. Construction of daily mosaic images.
7. Computation of ratio images, *i.e.* daily mosaic image *versus* the reference image.
8. Thresholding of ratio images to detect wet-snow. If the difference is more than 4 dB, the pixel is classified as wet-snow.
9. Masking of layover and shadow areas.

Currently, the algorithm supports Sentinel-1 GRD and Radarsat-2 SCN/SCW/SLC SAR images.

The benefit with this algorithm, compared to the one proposed in [12], is that we only need a single reference image for the area of interest. *E.g.* if the aim is to perform wet snow mapping for the whole of Romania, the reference image would cover the whole country, and will be constructed by averaging daily mosaic image for the snow-free months.

### 3. RESULTS

The algorithm test results for the sites in Romania are presented in the following. The results are here limited to comparison with air temperature for the 2015 winter season, but will be extended with comparison with *in situ* snow wetness measurements and the use of Sentinel-3 data when these become available for the 2017 season.

#### 3.1. OPTICAL SNOW WETNESS

The optical snow wetness products have been generated using the time series of Terra MODIS data acquired from 1 January 2015 to 30 June 2015 for the study area represented by the upper parts of the Arges and Ialomita Rivers Catchments.

Using MODIS data give the resolution of the OWS retrieval products of 1 km<sup>2</sup>. In order to present the temporal dynamics and development of the snow conditions a number of *optical snow wetness* (OWS) products have been selected. The less-to-no cloud cover images have been selected and is presented in Table 1.

For the OWS analysis only Fundata, Sinaia 1500, Bâlea Lac and Vf. Omu weather stations have been taken into consideration because the other stations are within forested and urban areas. The altitude gradient in the melting season is well covered by the four stations. On the other hand, because Fundata and Sinaia 1500 are situated very close to the forest limit, the neighbour pixels in the east of Fundata and west of Sinaia 1500 had to be used. It means that there might be differences due to the slight variation in altitude for air temperatures close to 0 °C.

Table 1

OSW map retrieval results (W) and corresponding air temperature measurements in the morning (08:00), closest to the acquisition time (Ac) and in the afternoon (14:00) for the four weather stations. All times are given in UTC. The retrieval results are shown colour coded as well as with letters (D = Dry, M = Moist, W = Wet, V = Very wet and S = Soaked snow). When there is no OSW retrieval result, other classes are shown ('+' = Cloud, '-' = Partly snow-covered ground and '=' = Bare ground (no snow))

| Satellite ac. |      | Vf. Omu |       |       |       | Balea |       |       | Sinaia 1500 |   |       | Fundata |       |   |       |       |       |
|---------------|------|---------|-------|-------|-------|-------|-------|-------|-------------|---|-------|---------|-------|---|-------|-------|-------|
| Date          | Time | W       | 8:00  | Ac    | 14:00 | W     | 8:00  | Ac    | 14:00       | W | 8:00  | Ac      | 14:00 | W | 8:00  | Ac    | 14:00 |
| 17.01         | 9:00 | -       | -0.9  | 0.6   | -1.1  | -     | 2.6   | 2.5   | 2.7         | = | 8.2   | 10.1    | 8.5   | = | 4.8   | 6.2   | 7.8   |
| 4.02          | 8:50 | +       | -13.9 | -14.1 | -12.7 | +     | -9.6  | -9.7  | -9.3        | + | -5.6  | -3.8    | -5.1  | - | -5.3  | -3.5  | -3.0  |
| 10.02         | 9:50 | +       | -20.8 | -19.7 | -19.7 | +     | -15.9 | -15.0 | -15.3       | - | -10.7 | -9.8    | -9.9  | - | -11.5 | -9.2  | -9.0  |
| 11.02         | 8:55 | D       | -20.8 | -20.6 | -20.4 | D     | -15.6 | -14.4 | -16.1       | - | -12.2 | -11.1   | -10.2 | - | -12.3 | -11.4 | -9.0  |
| 14.02         | 9:25 | D       | -8.7  | -7.0  | -7.0  | D     | -6.5  | -4.4  | -4.2        | - | 2.8   | 2.8     | -0.9  | - | 2.6   | 3.7   | 4.0   |
| 21.02         | 9:30 | D       | -2.2  | -3.1  | -3.3  | D     | -0.6  | 1.1   | -1.2        | D | -0.9  | 2.1     | 1.7   | W | -0.8  | 0.5   | 3.2   |
| 9.03          | 9:30 | D       | -1.7  | -0.8  | -2.3  | -     | 0.1   | 1.1   | -0.9        | D | 4.9   | 5.4     | 5.2   | - | 3.5   | 4.1   | 6.3   |
| 11.03         | 9:20 | +       | -4.6  | -3.5  | -5.2  | D     | -4.5  | -3.0  | -4.0        | D | -1.6  | 1.7     | 4.2   | = | -2.1  | 0.6   | 3.8   |
| 10.04         | 9:30 | D       | -9.0  | -7.6  | -4.9  | D     | 1.3   | 0.6   | 6.3         | - | 3.4   | 4.9     | 8.2   | S | 3.7   | 5.3   | 7.7   |
| 23.04         | 9:00 | D       | -8.9  | -7.7  | -2.2  | D     | -0.1  | -0.1  | 2.2         | - | 4.4   | 5.9     | 8.7   | = | 2.4   | 5.8   | 10.2  |
| 24.04         | 9:45 | -       | -2.0  | -0.1  | 0.8   | -     | 3.9   | 6.5   | 7.2         | - | 10.2  | 13.7    | 13.2  | = | 10.5  | 12.5  | 14.0  |
| 25.04         | 8:50 | -       | 0.7   | 1.3   | 2.4   | -     | 5.3   | 6.7   | 6.7         | = | 13.0  | 13.5    | 11.2  | = | 13.2  | 14.0  | 13.5  |
| 20.05         | 8:40 | =       | 8.1   | 8.9   | 6.8   | -     | 11.0  | 10.6  | 9.4         | = | 18.5  | 19.0    | 15.5  | = | 17.2  | 18.8  | 16.5  |
| 6.06          | 9:25 | =       | 5.9   | 8.3   | 8.5   | -     | 10.3  | 10.8  | 12.5        | = | 15.0  | 17.8    | 17.0  | = | 14.5  | 15.8  | 18.5  |
| 15.06         | 9:20 | =       | 7.2   | 9.6   | 10.8  | +     | 12.6  | 14.1  | 10.9        | + | 12.6  | 19.5    | 18.4  | = | 16.0  | 18.3  | 15.0  |

After the third maximum accumulation recorded on 8<sup>th</sup> and 9<sup>th</sup> of April 2015 at Bâlea Lac weather station (243 cm), the snowmelt season begins at medium-to-low altitudes. The map in Fig. 2 shows that, at lower altitudes (less than 1500 m a.s.l.) in south-oriented slopes the melting is faster also because positive temperatures are much more extensive during the day. It is not the same situation at higher altitudes where the snow is still dry and the temperatures are negative all day long at Vf. Omu and positive only few hours at Bâlea Lac weather station as illustrated in Fig. 3.

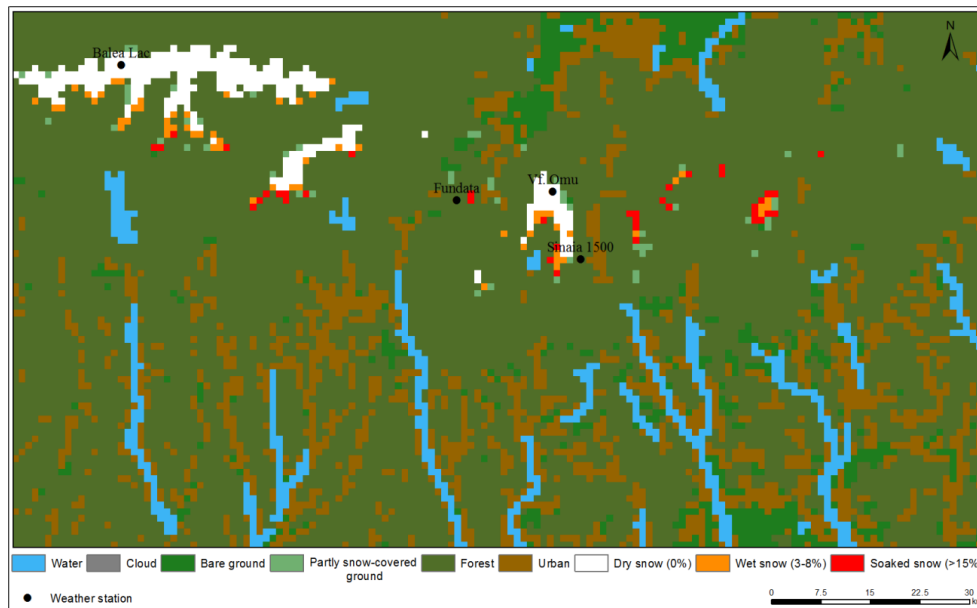


Fig. 2 – Optical snow wetness based on MODIS from 10 April 2015 acquired at 09:30 UTC.

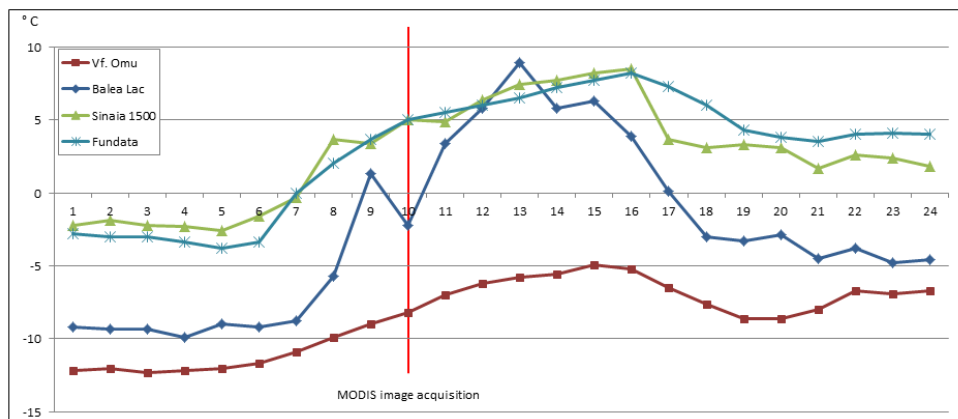


Fig. 3 – Temperature profiles at weather stations on 10 April 2015.

### 3.2. SAR SNOW WETNESS

The hourly air temperatures, around the satellite passage, at weather stations together with SWS results are listed in Table 2. All times are given in UTC and the image acquisition in the afternoon (around 16.30), ascending pass. The hourly air temperatures are used for making the difference between the dry snow and the bare

ground, which are included in the same class. Most of the analysed images (coloured in light green) are classified as dry snow or bare ground.

Table 2

SWS map retrieval results (Ac) and corresponding air temperature measurements closest to the acquisition time for the four weather stations. All times are given in UTC.

The results are shown colour coded as well as with letters

(W = Wet snow, DB = Dry snow or bare ground)

| Satellite ac. | Vf. Omu |       |       | Bălea Lac |       |       | Sinaia 1500 |       |       | Fundata         |       |       |
|---------------|---------|-------|-------|-----------|-------|-------|-------------|-------|-------|-----------------|-------|-------|
| Date          | Ac      | 16:00 | 17:00 | Ac        | 16:00 | 17:00 | Ac          | 16:00 | 17:00 | Ac              | 16:00 | 17:00 |
| 30.01         | DB      | -9.1  | -9.3  | DB        | -5.4  | -5.3  | DB          | -2.8  | -2.3  | DB              | -0.5  | -0.4  |
| 23.02         | DB      | -4.0  | -4.2  | DB        | -1.1  | -1.8  | DB          | 1.0   | 0.5   | DB              | 2.0   | 1.9   |
| 19.03         | DB      | -14.7 | -15.2 | DB        | -11.8 | -11.6 | DB          | -6.6  | -7.8  | DB              | -4.8  | -5.5  |
| 31.03         | W       | -7.5  | -7.9  | DB        | -2.4  | -1.1  | DB          | 2.0   | 1.7   | DB              | 4.6   | 3.6   |
| 12.04         | DB      | -0.4  | -1.4  | DB        | 2.6   | 1.2   | DB          | 8.1   | 8.0   | DB              | 11.0  | 9.7   |
| 24.04         | DB      | 0.2   | -0.4  | DB        | 4.9   | 4.0   | DB          | 8.6   | 7.8   | DB              | 13.4  | 11.5  |
| 6.05          | DB      | 6.7   | 6.3   | DB        | 11.7  | 11.7  | DB          | 12.2  | 12.1  | DB              | 15.8  | 15.0  |
| 18.05         | DB      | 5.2   | 4.2   | DB        | 6.3   | 5.8   | DB          | 12.2  | 10.2  | DB              | 15.0  | 14.0  |
| Satellite ac. | Predeal |       |       | Câmpulung |       |       | Câmpina     |       |       | Curtea de Argeş |       |       |
| Date          | Ac      | 16:00 | 17:00 | Ac        | 16:00 | 17:00 | Ac          | 16:00 | 17:00 | Ac              | 16:00 | 17:00 |
| 30.01         | DB      | 1.7   | 1.5   | DB        | 4.0   | 3.8   | DB          | 2.2   | 2.6   | DB              | 5.9   | 5.6   |
| 23.02         | DB      | 3.9   | 2.7   | DB        | 6.5   | 6.0   | DB          | 5.9   | 5.8   | DB              | 7.9   | 7.2   |
| 19.03         | DB      | -3.6  | -3.7  | DB        | 0.9   | 0.0   | DB          | 0.1   | -0.6  | DB              | 2.5   | 1.2   |
| 31.03         | DB      | 5.6   | 4.9   | DB        | 10.3  | 8.8   | DB          | 13.1  | 11.4  | DB              | 10.1  | 9.1   |
| 12.04         | DB      | 13.7  | 9.9   | DB        | 17.9  | 16.0  | DB          | 18.5  | 15.4  | DB              | 18.8  | 17.8  |
| 24.04         | DB      | 15.3  | 13.8  | DB        | 18.7  | 17.3  | DB          | 18.9  | 17.2  | W               | 20.7  | 18.4  |
| 6.05          | DB      | 17.4  | 16.7  | DB        | 20.7  | 20.0  | DB          | 20.3  | 19.6  | DB              | 23.4  | 22.5  |
| 18.05         | DB      | 18.8  | 16.8  | DB        | 21.0  | 20.3  | DB          | 21.7  | 20.6  | DB              | 22.8  | 21.6  |

In Fig. 4 we show the SAR wet snow (SWS) map for the test site for 12 April 2015. Light blue areas correspond to wet snow, green to dry snow or bare ground, blue areas to water bodies, purple to SAR shadow areas, and dark grey to areas outside the satellite coverage.

Figure 5 shows temperature profiles for six meteorological stations with corresponding wet snow map for the test site on April 12<sup>th</sup> 2015. The Campulung and Curtea de Argeş weather station are not included as they have not 24 hours measurement program. Vf. Omu weather station is located close to very steep terrain on a mountain peak. On April 12<sup>th</sup> the dry snow is dominant around the stations, due to negative or close to 0 °C temperatures at the image acquisition hour. At the same date, at Bălea Lac dry snow dominated the surface around the station due to the fact that this is located on the northern slope. So, even though the temperatures are positive, the snow is dry. All the other stations have temperatures close to or above 0 °C, so the retrieval results that there is bare ground is probably correct.

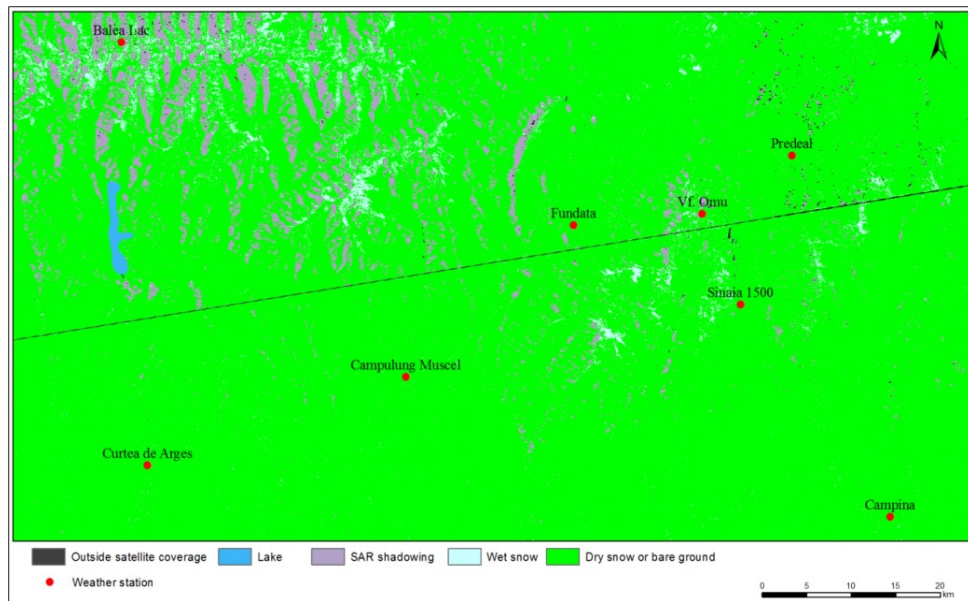


Fig. 4 – SAR wet snow map for the validation area on 12 April 2015.

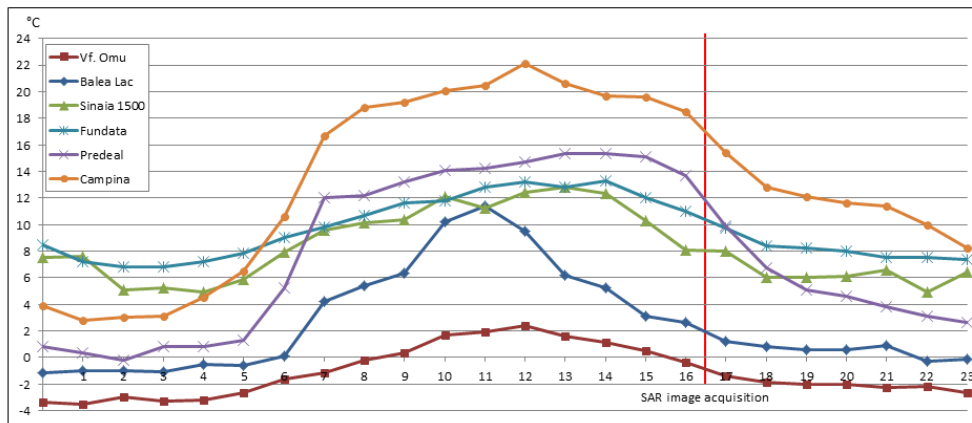


Fig. 5 – Temperature profiles at weather stations on 12 April 2015.

#### 4. DISCUSSION AND CONCLUSIONS

Algorithms for single-sensor wet snow mapping based on optical and SAR data were tested and improved. The primary data sources for SAR and optical are Sentinel-1 and Sentinel-3, respectively, but due to lack of Sentinel-3 data Terra MODIS was used in this study. The algorithms and products have been through the

first stage of tests, including calibration and validation based on *in situ* measurements.

The products are foreseen to be applied with hydrological modelling for flood prediction and for snow avalanche applications. They might be applied as part of the data basis for making warnings of snow avalanche hazards, and they might also be used for the detection of potential weak snow layer formation during the snow accumulation season.

The test results for sites in Romania for the 2015 season have been presented. The validation was limited to comparison with air temperature as this was what was available for the 2015 season, but will be extended with comparison with *in situ* snow liquid water measurements and the use of Sentinel-3 data when these become available for the 2017 season. Data from eight stations were available, and a comparative analysis between air temperature measurements and satellite products were carried out.

The analysis of the retrieval results for snow wetness from optical data confirmed that the approach of combining snow surface temperature and snow grain size, analysed in a time series of observations, can be used to infer wet snow. Air temperature measurements from meteorological stations confirm in general the maps produced. In most cases retrieval results of dry snow corresponded with air temperatures below freezing point, and retrieval results of one of the wet-snow classes with air temperatures above freezing point. The highest temperatures usually gave the wettest snow classes. When inconsistencies were identified, most could be well explained with transitions from cold and dry conditions during the night to wet snow at some time during the day. If air temperatures above 0 °C have lasted for a short time (up to 2–3 hours), the snow surface has not necessarily become wet. What happens when the air temperature is above freezing point depends very much on the wind. The melting intensity strongly increases with wind speed for air temperatures above 0 °C.

The OWS maps are also internally consistent in the way that the content usually follows the topography and local climate very well and without being noisy. The temporal transitions are similar in the way that increasing temperatures gives increasing wetness, also within the same day (for the cases when we had more than one snow map from the same day). Increasing temperature during the day at lower altitudes also consistently brings wet snow to higher altitudes. Also, the classes follow the topography logically (canonically) with wettest snow at lower altitudes and reduced wetness with altitude.

Furthermore, C-band SAR data is very sensitive to whether the snow is wet or dry, which was confirmed in our work. However, C-band alone cannot be used to determine the degree of wetness. The use of flattening gamma terrain correction reduces the terrain effects substantially, and we may therefore create daily mosaics by combing ascending and descending satellite passes. However, for mapping of wet snow, this may not be desirable since the snow wetness varies between night

and day due to varying temperatures. We have therefore chosen only to consider the afternoon (ascending) passes.

Only using air temperature as a proxy for *in situ* measured snow wetness is of course a limitation, and the classes in the maps do most likely diverge from their definition in terms of liquid water content. Proper calibration of the algorithms will be done using data from the cal/val sites and field campaigns from the 2016 and 2017 seasons.

Some of the wet snow maps for Romania seem to underestimate the snow-covered area, in some cases seriously. As the OWS algorithm require an area to have almost 100% snow cover fraction to be able to retrieve the snow wetness, also the area of wet snow gets underestimated in these cases. The problem is probably related to the lack of specific calibration and adaptation of the Norwegian algorithms to Romania. However, we have not yet understood the exact cause. It might be related to systematic differences between the two countries. The problems are expected to be mitigated when we obtain data from the new cal/val sites in Romania in the 2017 winter and spring season.

In conclusion, the results presented here have in general confirmed that our approach of combining snow surface temperature and snow grain size, analysed in a time series of observations, can be used to infer wet snow. When combined with SAR observations of wet snow, snow wetness maps should be obtainable frequently (with daily maps as a goal). With both Sentinel-1A and -1B available with full performance of delivery in 2017 and both Sentinel-3A and -3B available in 2018, we expect to be able to produce close-to-daily snow wetness maps. Final adaptation and validation for Sentinel-3 will take place as soon as these data are available.

*Acknowledgements.* The research leading to these results has received funding from EEA Financial Mechanism 2009–2014 under the SnowBall project, contract 19SEE/2014.

#### REFERENCES

1. P. Lemke *et al.*, Observations: Changes in Snow, Ice and Frozen Ground, *Climate Change 2007: The Physical Science Basis*, 4<sup>th</sup> Assessment Report of IPCC, Cambridge Univ. Press, 337–383 (2007).
2. M. C. Serreze *et al.*, *Observational evidence of recent change in the northern high-latitude*, *Climatic Change* **46**, 159–207 (2000).
3. R. O. Green, T. H. Painter, D. A. Roberts and J. Dozier, *Measuring the expressed abundance of the three phases of water with an imaging spectrometer over melting snow*, *Water Resources Research* **42**, W10402 (2006).
4. R. Solberg, J. Amlien, H. Koren, L. Eikvil, E. Malnes and R. Stovold, *Multi-sensor/multi-temporal analysis of ENVISAT data for snow monitoring*, *Proceedings of ESA ENVISAT & ERS Symposium* (2004).
5. J. R. Key, J. B. Collins, C. Fowler and R. S. Stone, *High-latitude surface temperature estimates from thermal satellite data*, *Remote Sensing of Environment* **61**, 302–309 (1997).

6. J. Amlien and R. Solberg, *A comparison of temperature retrieval algorithms for snow covered surfaces*, Proceedings of the International Geoscience and Remote Sensing Symposium (2003).
7. J. Stroeve, M. Haefliger and K. Steffen, *Surface temperature from ERS-1 ATSR infrared thermal satellite data in polar regions*, Journal of Applied Meteorology **35**, 1231–1239 (1996).
8. C. Coll, V. J. Caselles, A. Sobrino and E. Valor, *On the atmospheric dependence of the split-window equation for land-surface temperature*, International Journal of Remote Sensing **15**, 105–122 (1994).
9. J. Dozier, *Spectral signature of alpine snow cover from the Landsat Thematic Mapper*, Remote Sensing of Environment **28**, 9–22 (1989).
10. M. Fily, B. Bourdelles, J. P. Dedieu and C. Sergent, *Comparison of In Situ and Landsat Thematic Mapper Derived Snow Grain Characteristics in the Alps*, Remote Sensing of Environment **59**, 452–460 (1997).
11. R. Solberg, H. Koren, J. Amlien, E. Malnes, D. V. Schuler and N. K. Orthe, *The development of new algorithms for remote sensing of snow conditions based on data from the catchment of Øvre Heimdalsvatn and the vicinity*, Hydrobiologia **642**, 35–46 (2010).
12. T. Nagler and H. Rott, *Retrieval of wet snow by means of multitemporal SAR data*, IEEE Transactions on Geoscience and Remote Sensing **38**, 754–765 (2000).
13. D. Small, *Flattening gamma: Radiometric terrain correction for SAR imagery*, IEEE Transactions on Geoscience and Remote Sensing **40**, 3081–3093 (2011).